Reconstruction of cloud geometry from multi-view satellite images

Gabriela Seiz [a,*], Roger Davies [b]

[a] Institute of Geodesy and Photogrammetry, Swiss Federal Institute of Technology ETH, ETH-Hoenggerberg, 8093 Zürich, Switzerland
[b] Jet Propulsion Laboratory, California Institute of Technology, 4800 Oak Grove Drive, Pasadena, CA 91109, USA

Abstract

Reflected solar radiances measured by the pushbroom cameras of the Multiangle Imaging SpectroRadiometer (MISR) on the Terra satellite at nine viewing angles are combined to give eight stereo pairs. These are analyzed with stereo-photogrammetric methods to measure the geometry of a convective cloud system. Both cloud-top heights and cloud sides are retrieved with a precision of about 200 – 300 m. Two case studies of deep, convective clouds over ocean are considered. The accuracy of the MISR retrieval is tested in the first case study by reference to coincident, higher resolution stereo data from ASTER, showing how the accuracy of the cloud-top height retrieval is improved using the oblique MISR views. In the second case study, the entire cross-section of the cloud aligned with the viewing azimuthal direction is measured, using all nine cameras. The methodology presented is an important step towards more routine retrievals of the 3D geometrical reconstruction of isolated, deep-convective clouds. Such reconstructions are a necessary prerequisite to the subsequent 3D radiative transfer modeling used to aid the remote sensing of the elusive microphysical properties of such clouds.
© 2005 Elsevier Inc. All rights reserved.

Keywords: Atmosphere; Clouds; Multi-view; Photogrammetry; Radiative transfer

1. Introduction

The relationship between cloud radiative properties (e.g. albedo) and their hydrological properties (e.g. water content) is a crucial component of satellite remote sensing and climate modeling. For many types of cloud around the world, this relationship depends strongly on the nature of cloud heterogeneity and on whether the reflectivity is saturated. Heterogeneity prevents application of conventional one-dimensional radiative transfer models, and when saturation occurs, all that can be said about cloud water amount is that it exceeds the value required for saturation. Trustworthy relationships between cloud radiation and hydrology are therefore limited to thinner clouds that do not suffer from brightness saturation, and that exhibit an adequate degree of horizontal homogeneity. As noted in earlier studies (Genkova & Davies, 2003; Horváth & Davies, 2004; Loeb & Davies, 1996), the majority of clouds do not meet these constraints.

The realm of heterogeneous cloud suffering from brightness saturation is perhaps best typified by deep, convective clouds.

These are dominated by a three-dimensional structure, often with vertical extents greater than their horizontal dimension, and can be extremely reflective. Here we explore the remote sensing of such clouds by posing the simplest question: how well can we resolve the main features of their geometry from space? This is a desirable prerequisite before attempting a full 3D radiative transfer solution to retrieve the internal cloud properties, although in an earlier study using MISR data, Zuidema et al. (2003) showed promising results using reconstructions based primarily on operational cloud-top heights. Our motivation to answer this question also stems from the recent availability of novel multiangle measurements of cloud reflectivity from the Multiangle Imaging SpectroRadiometer (MISR) on the Terra satellite, from which it appears that geometrical reconstructions of cloud-top heights and cloud sides should be possible using pairs of viewing angles in different stereo combinations. From an operational perspective, that is affected by the dual requirements of computational speed and adequate global coverage, the MISR data products already use two near-nadir stereo pairs to determine cloud-top height at a horizontal resolution of 1.1 km, with an rms uncertainty in height of about 550 m (Moroney et al., 2002), and a combination of two other stereo pairs to retrieve the height-resolved mesoscale wind components at a horizontal

* Corresponding author.
   E-mail address: gabriela.seiz@esa.int (G. Seiz).

resolution of about 70 km (Horváth & Davies, 2001). The extension of these techniques to full resolution reconstructions of the type discussed here is considerably beyond the current operational capability, and must be tackled as a special study.

We proceed by identifying two examples of deep, convective clouds in the MISR data set. The first is a rare example for which data are also available from the ASTER instrument (also on Terra) at considerably higher spatial resolution, but for only two viewing directions. This case study addresses the limitations imposed on identifying stereo features due to MISR's lower resolution. The second case study is of a particularly well-defined convective cloud for which both sides are visible during the Terra overpass, and for which we attempt the reconstruction of a complete cross-section using eight different viewing angle pairs. To our knowledge, this is the first such stereo-photogrammetric reconstruction of cloud geometry from space.

2. Data

We used data measured by the MISR and ASTER instruments onboard the NASA EOS-Terra spacecraft, launched in December 1999. The Terra orbit is sun-synchronous at a mean height of 705 km, with an inclination of 98.5° and an equatorial crossing time of about 10:30 am local solar time. The repeat cycle is 16 days. In the following two paragraphs, the data characteristics of MISR and ASTER are explained.

2.1. MISR

The MISR instrument consists of nine pushbroom cameras, labeled Df, Cf, Bf, Af, An, Aa, Ba, Ca, and Da, from the most forward oblique view, through nadir, to the most oblique backward view. The corresponding viewing zenith angles are: 70.5° (Df, Da), 60° (Cf, Ca), 45.6° (Bf, Ba), 26.1° (Af, Aa) and 0° (An). The time delay between adjacent camera views of the same scene is 45–60 s, which results in a total delay between the Df and Da images of about 7 min. Of the four MISR spectral bands, only the red (672 nm) band was used in this study. The red-band data from all nine cameras are saved at high-resolution, sampled at 275 m × 275 m, consistent with the average pixel size. The operational data products from MISR are described in Lewicki et al. (1999). The product used for this study is the L1B2 ellipsoid-projected radiance data product, which is referenced to the surface of the WGS84 ellipsoid with no terrain elevation included. The spatial horizontal accuracy requirements of the MISR georectified product are driven by the needs of the geophysical parameter retrieval algorithms. The goal of operational MISR data processing is to achieve an uncertainty better than ±140 m for both the absolute geolocation of the nadir camera and the coregistration between all nine cameras (Jovanovic et al., 2002). The detailed theory on the georectification algorithms and the in-flight camera geometric model (CGM) calibration is described in Jovanovic et al. (1999a) and Jovanovic et al. (1999b). The latest evaluation results for CGM versions 6 and 7 shown in Jovanovic et al. (2002) are approaching prelaunch requirements, with along- and across-track errors far below 1 pixel for all cameras, except for the Da

camera. The Da camera experiences some larger registration errors that occasionally reach a few pixels, the source of which remains obscure. While these errors will be corrected in future versions (F03_0024 onwards) on the MISR operational product, our study predates this correction, and we simply use caution in interpreting the influence of the Da camera.

2.2. ASTER

The Advanced Spaceborne Thermal Emission and Reflection Radiometer (ASTER) is an advanced multispectral imager that covers a wide spectral region with 14 bands from the visible to the thermal infrared with high spatial, spectral and radiometric resolution (Yamaguchi et al., 1998). The visible-near-infrared (VNIR) subsystem, which provides the stereo images in channel 3 (i.e. 3N/3B at 820 nm), consists of two independent telescope assemblies in the backward (i.e. −27.6°) and nadir view directions and has a spatial resolution of 15 m. A time lag of about 55 s occurs between the acquisition of the nadir and backward images. Each ASTER scene covers an area of 60 km × 60 km. In contrast to all other sensors on EOS-Terra (i.e. MISR, MODIS, CERES), ASTER does not acquire data continuously due to the huge amount of data it generates, but only on specific dates/orbits (i.e. on demand). The L1B data product used in this study is projected into the Universal Transverse Mercator UTM (default) or Space Oblique Mercator SOM projection (Snyder, 1987), with a grid spacing of approximately the full instrument resolution, i.e. 15 m for the 3N/3B VNIR image data, with a radiometric resolution of 8-bit. The ASTER images are geolocated with an accuracy of about 1–2 pixels on average, or 15–30 m. So, with the ASTER data simultaneous to MISR, we have a reference data set for cloud geometry retrieval with about 5 times better accuracy than MISR (i.e. 30 m versus 140 m) (Seiz, 2003; Seiz et al., accepted for publication).

3. Cloud geometry retrieval

The nine viewing angles of MISR provide a good view of the cloud top, as well as the cloud sides as far as they are visible in the along-track flight direction, forward and backward. As the cloud shapes and subsequent modeling are very complex, when considering the full 3D structure, we have concentrated in this preliminary study on measuring just the cross-section of an isolated, deep-convective cloud. Consequently, the most optimal measurement strategy is to take the cross-section line approximately parallel to the along-track direction.

For the retrieval of the cross-section geometry, the center point of each pixel along the cross-section line was used in the matching process (Seiz, 2003), which is briefly described as follows. First, all MISR images were reduced to 8-bit with linear stretching between the minimum and maximum values. As no a priori values of the cloud heights were given to the matching algorithm, the number of pyramid levels for the hierarchical matching was chosen so that the maximum possible parallax at the highest level was only 3–4 pixels. Three pyramid levels were used. Every pyramid level was then enhanced and radiometri-

cally equalized with a Wallis filter (Wallis, 1976; Baltsavias, 1991). The unconstrained Multi-Photo Geometrically Constrained (MPGC) least-squares matching (LSM) algorithm (Grün, 1985; Baltsavias, 1991) was applied hierarchically, starting on the highest pyramid level. After each pyramid level, quality control with absolute tests on the LSM matching statistics was performed to exclude the largest blunders from further processing down the pyramid. The patch size was increased from one pyramid level to the next, from 7×7 on the highest level to 15×15 on the lowest level. After applying the MPGC LSM algorithm, the matching solutions on the lowest level were quality-controlled with absolute and relative tests on the matching statistics. The matched points were converted into cloud-top heights by forward intersection of the viewing rays, defined by the satellite position at pixel acquisition time and the apparent cloud location on the Earth (i.e. ellipsoid). It was assumed that there is no significant cloud motion within the 7-min interval of the MISR image acquisition, which is a realistic assumption for this cloud type. As the target areas were located over ocean, with no nearby coast lines or other landmarks which could be used as ground-control points, we were not able to check the accuracy of the operational geolocation data.

It is important to note that with this automated matching procedure, a continuous surface of the object (i.e. cloud) within the patch is assumed. Therefore, any sharp discontinuities are either smoothed or fail to be matched. In addition, as the patch size cannot be smaller than a certain minimum size (i.e. about 7×7 pixels), the difficulties will be enhanced for smaller object structures.

4. Results

For the selection of the two case studies, the MISR orbits since launch in December 1999 were screened for isolated, deep-convective clouds over ocean, with sufficient illumination of the two visible cloud sides. For the first case, an additional search criterion was the presence of ASTER data for the region of interest.

4.1. Case 1

Case 1 was acquired on 8 July 2004 (path 97, orbit 24227). The region of interest spans 147.1–147.4°E, 2.4–2.6°S. Here,

Table 1
Cloud top (i.e. max height) and base (i.e. min height) height results for four backward view combinations

	An–Aa	Aa–Ba	Ba–Ca	Ca–Da
Max height (m)	5617	8719	8602	9064
Min height (m)	2034	1949	1918	2314

the solar illumination is from the top, right-hand side of the image (i.e. azimuth angle of 41.1°) and a zenith angle of 34.2°, so that the backward views tend to see the shadowed side of the cloud. As the dimension of this cloud is relatively small, points could be matched manually in the different views. Manual measurement of object points in several views is most convenient and accurate within a photogrammetric workstation, which allows the scene to be viewed in stereo. Unfortunately, the functions to import MISR into a commercial photogrammetric workstation (e.g. Leica LPS) were not available, so that the manual measurements had to be done in a simple image-processing tool (allowing at least to zoom accordingly and to arrange the images next to each other). In Fig. 1, the nadir and the four backward views of the convective cloud are shown, overlaid with the location of the manually measured points. The height results from the four backward viewing combinations (listed in Table 1) show that the base height of this cloud of about 2.0 km could already be retrieved with the inner-most view combination (i.e. An–Aa), while the cloud-top height of the small cloud 'peaks' at up to about 8–9 km is substantially underestimated by this An–Aa view combination. The base and top heights of the other three MISR view combinations (i.e. Aa–Ba, Ba–Ca and Ca–Da) are consistent, with Ca–Da slightly different. The underestimation of the top heights in the An–Aa view combination occurs because of the small cloud features at cloud top which are not visible enough in the near-nadir views at the MISR spatial resolution of 275 m. To confirm the top height of the small cloud features, the stereo images of ASTER were analyzed. As illustrated in Fig. 2, the ASTER images with a spatial resolution of 15 m show a lot more detail of the convective cloud structure. The retrieved cloud-top heights of three distinct small cloud features at 8.6, 8.4 and 7.3 km are well in accordance with the values retrieved from MISR's view combinations (except An–Aa). In this context, ASTER images proved to be very useful to explain
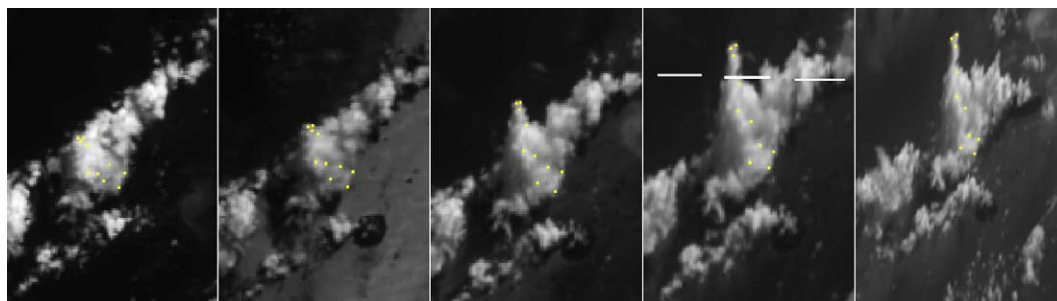

Fig. 1. Deep convective cloud over ocean, MISR scene on 8 July 2004, Path 97, Orbit 24227, blocks 9194. From left to right: An view, Aa view, Ba view, Ca view, Da view. Yellow: manually measured cloud points.
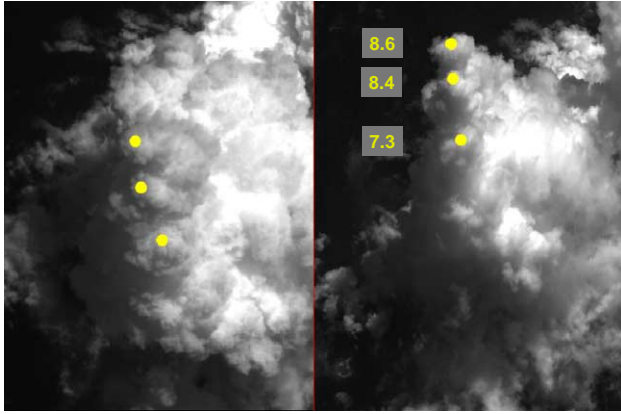
Fig. 2. Manual matching results (yellow) of small features at cloud top, as seen by ASTER's nadir (left) and backward (right) view. The plotted cloud-top height results are in km.

the retrieval differences between the various MISR view combinations.

The results are also consistent with the cloud-top height value of 8.6 ± 0.5 km from the operational MODIS MOD06 cloud-top pressure (CTP) product (Menzel et al., 2002). For the pressure to height conversion, a nearby sounding was used. However, it has to be noted that the MODIS MOD06 CTP product has a horizontal resolution of 5×5 km only, so this CTH value is an average value over the 5 km region and cloud changes at higher spatial resolution cannot be resolved by the MODIS product.

4.2. Case 2

Case 2 was acquired on 2 September 2003 (path 78, orbit 19726) with a solar zenith angle of $21.3°$. The region of interest spans $177.2–177.4°E$, $5.2–5.8°N$. In Fig. 3, the nadir and the two most oblique views of the convective cloud are shown. These are plotted as measured, with constant sampling, and have not been adjusted to provide a perspective view. Consequently, the vertical sides appear more stretched than they would to a human observer. Solar illumination is from the right of the images, with little direct illumination of the cloud sides.

As described in Section 3, a cross-section line was defined approximately parallel to the along-track direction, illustrated

in Fig. 3. The center point of each pixel on the cross-section line was then pairwise matched in eight different view combinations, i.e. Cf–Df, Bf–Cf, Af–Bf, An–Af, An–Aa, Aa–Ba, Ba–Ca and Ca–Da. In Fig. 4, the resulting heights of the cloud points of each view combination are plotted against the UTM y-coordinate. The Cf–Df combination, as well as the Bf–Cf combination retrieves the forward cloud side and some points at the cloud top. The inner camera combinations Af–Bf, An–Af and An–Aa then mainly show points along the cloud top. Starting from Aa–Ba, the aft viewed geometry of the cloud is measured. While the results from Aa–Ba and Ba–Ca are consistent, the heights from Ca–Da are different from the other 7 viewing combinations, which is most likely caused by geolocation problems of the Da camera. As mentioned earlier, the region of interest is over ocean and no nearby landmarks (e.g. coast lines) were therefore measurable to effectively determine the geolocation accuracy. Fig. 5 gives an impression how well the 3D points from the different view combinations coincide with each other. Because of the different results of the Ca–Da combination and the known geolocation problems of Da mentioned before, only the other seven view combinations were used for this plot. In Table 2, the vertical and horizontal (i.e. in along-track direction) accuracies are listed for the eight view combinations. These accuracies have been calculated from the viewing geometry, with assuming a matching accuracy of ± 0.5 pixels of our cloud matching procedure as validated in Seiz (2003). Overall, taking all camera pairs (except Ca–Da) into account, the cloud geometry can be retrieved with an accuracy in the order of $\pm 200–300$ m. For the cloud sides, the horizontal uncertainty of up to ± 220 m depends mainly on the oblique view combinations with larger horizontal along-track errors, as the near-nadir views have more difficulty seeing the side due to obscuration by the top. The vertical position of the cloud top and sides is most precisely determined by the more oblique view combinations with increased base-to-height ratios, i.e. ± 130 m for Cf–Df versus ± 280 m for An–Af/An–Aa, respectively. It has to be noted that the accuracies in Table 2 only take into account the viewing geometry and the matching accuracy; they do not include any additional errors (e.g. geolocation errors) which can add further uncertainties to the common cloud geometry. In our case, we can see in Figs. 4 and 5 that the largest CTHs vary between about 7.8 km (Af–Bf) and 8.7 km (Aa–Ba, Ba–Ca),
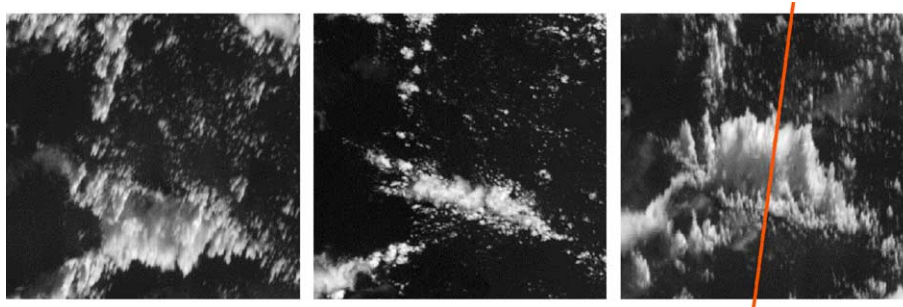

Fig. 3. Deep convective cloud over ocean, MISR scene on 2 Sep 2003, Path 78, Orbit 19726, blocks 83–86. Left: Df view, center: An view, right: Da view (red: cross-section line through the convective cloud).
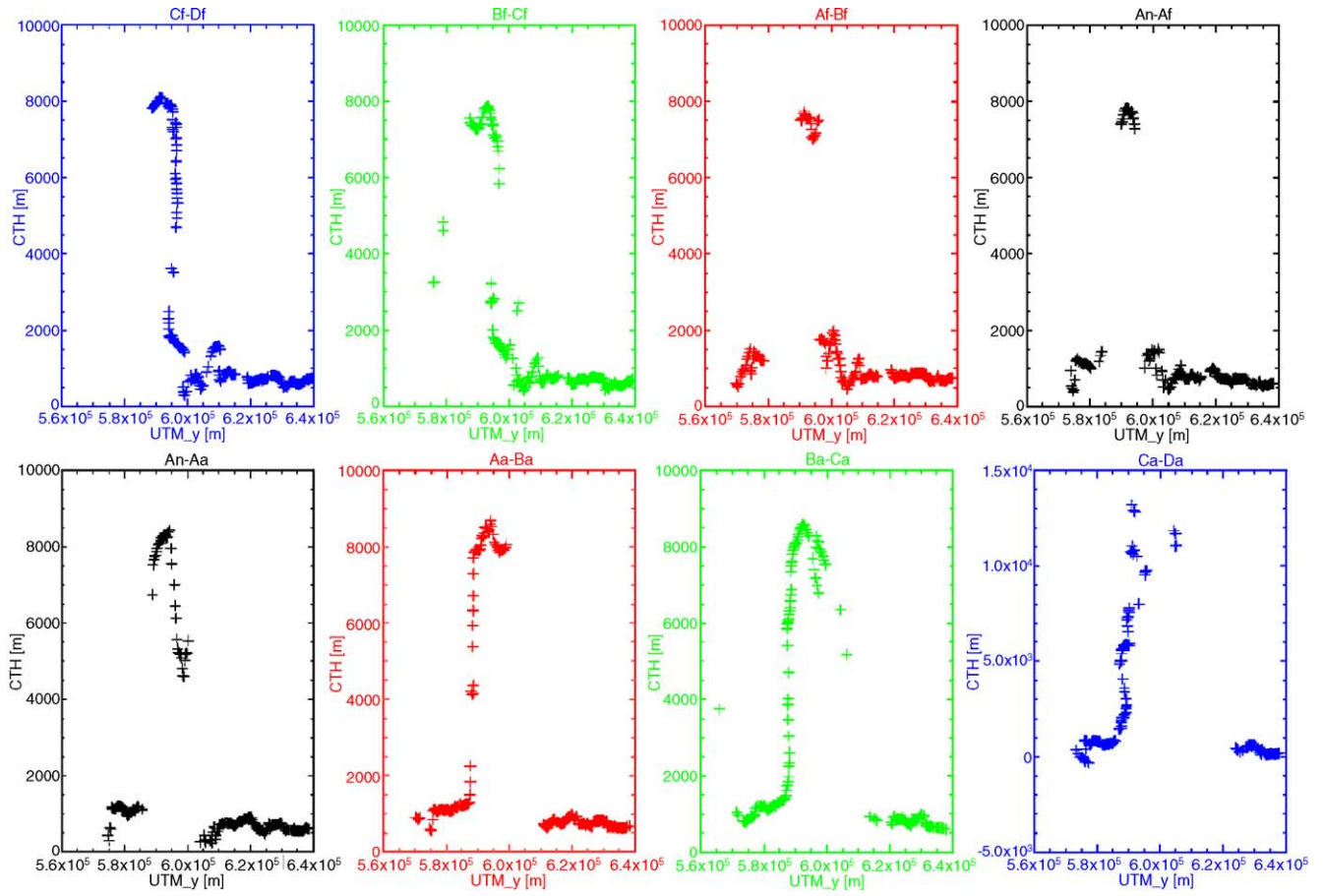
Fig. 4. Height results of cloud points along the cross-section line, shown in Fig. 3, for each of the 8 view combinations.
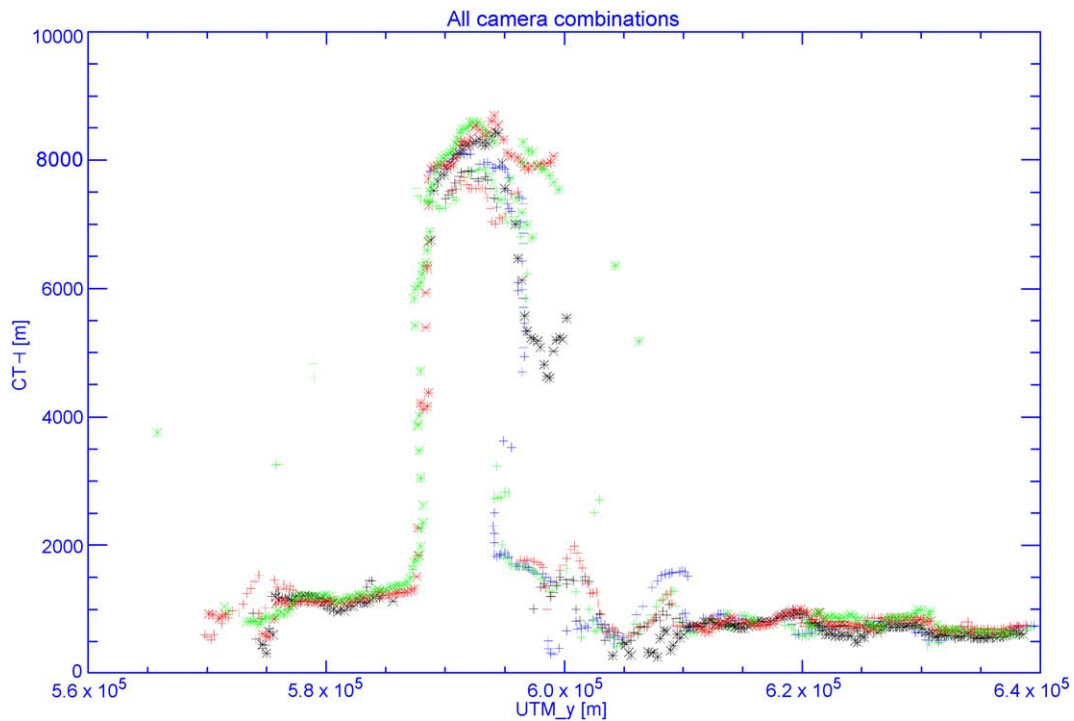

Fig. 5. Combined plot of all view combinations (except Ca–Da), showing the consistent height results of the cloud points along both visible cloud sides as well as at the cloud top.

Table 2
Vertical and along-track horizontal accuracy, assuming a matching accuracy of ±0.5 pixels

View combination	Vertical accuracy (i.e. CTH) (m)	Horizontal along-track accuracy (i.e. y) (m)
An–Af	281	0
An–Aa		
Af–Bf	259	127
Aa–Ba		
Bf–Cf	193	198
Ba–Ca		
Cf–Df	126	218
Ca–Da		

which is slightly larger than can be explained by the viewing geometry and matching accuracy only and is most probably mainly caused by remaining geolocation errors (i.e. in the order of 0.5 to 1 pixels) between the views.

The MODIS CTH from the operational MOD06 product is 8.1±0.5 km for this case, so again consistent with our MISR retrievals.

5. Conclusions

In this paper, we have presented the use of MISR onboard EOS-Terra for 3D geometric reconstruction of isolated deep convective clouds over ocean. In particular, we have outlined the unique opportunity with MISR, thanks to its nine viewing angles, to continuously scan the forward cloud side, then the cloud top structure and finally the backward cloud side in along-track direction during the overflight. As these clouds have very complex structures, with many discontinuities, automated matching is not sufficient to retrieve a good approximation of the full 3D geometry. A satisfactory result can only be achieved with complementary manual measurements, ideally using a photogrammetric workstation. As the import into a photogrammetric workstation was not yet possible for MISR, we have concentrated on manual measurements with a simple image processing tool for case 1, and on a cross-section retrieval along a defined line, approximately parallel to the along-track direction, for case 2. In the future, it would be interesting from a photogrammetric point of view to combine all available views and, if possible, some well-defined ground-control and tie points in a bundle adjustment to optimally estimate the 3D coordinates of the cloud points as well as to simultaneously determine any eventual systematic errors in the orientation data.

For case 1, the base height could be consistently retrieved by all four backward camera combinations, while the top height was consistently retrieved by the more oblique views only and substantially underestimated by the innermost view combination (i.e. An–Aa). The underestimation occurs because of the small cloud features at cloud top which are not visible enough in the near-nadir views of MISR. An advantage of the more oblique views of MISR is therefore clearly the ability to correctly retrieve the height of small cloud features ('peaks') around the cloud top. The use of the high-resolution ASTER stereo images for case 1 proved to be very helpful to verify the heights of these small structures at cloud top. For case 2, the results from the eight different viewing combinations nicely complemented each other to retrieve the full cross-section of the convective cloud. Only the Ca–Da combination was not used further, due to the rather large differences to the other seven camera combinations, probably caused by geolocation problems of the Da camera. After merging the various camera pairs, the relative accuracy of the cloud-top boundary is about 130–280 m vertically, dependent on the used view combinations, and that of the sides is about 200 m horizontally (along-track). The next step in our analysis, to be reported later, is to make immediate use of these results in a 3D radiative transfer model comparison against the measured radiance values, taking into account both the nominal cloud geometry, and the uncertainty in the cloud boundary locations, to constrain the retrieval of cloud properties.

Acknowledgements

References

Baltsavias, E. P. 1991, Multiphoto Geometrically Constrained Matching, Ph. D. dissertation, Institute of Geodesy and Photogrammetry, ETH Zurich, Mitteilungen No. 49, 221 pp.

Genkova, I., & Davies, R. (2003). Spatial heterogeneity of reflected radiance from globally distributed clouds. *Geophysical Research Letters*, *30*(21), 2096–2099.

Grün, A. (1985). Adaptive least squares correlation: A powerful image matching technique. *South African Journal of Photogrammetry, Remote Sensing and Cartography*, *14*(3), 175–187.

Horváth, A., & Davies, R. (2001). Simultaneous retrieval of cloud motion and height from polar-orbiter multiangle measurements. *Geophysical Research Letters*, *28*(15), 2915–2918.

Horváth, A., & Davies, R. (2004). Anisotropy of water cloud reflectance: a comparison of measurements and 1D theory. *Geophysical Research Letters*, *31*, 1102–1105.

Jovanovic, V., Lewicki, S., Smyth, M., Zong, J., & Korechoff, R. (1999a). MISR Level 1 Georectification and Registration. JPL Technical Report ATBD-MISR-03. Available at http://eospso.gsfc.nasa.gov/eos_homepage/for_scientists/atbd/docs/MISR/atbd-misr-03.pdf

Jovanovic, V., Smyth, M., & Zong, J. (1999b). MISR Level 1 In-flight Geometric Calibration. JPL Technical Report ATBD-MISR-04. Available at http://eospso.gsfc.nasa.gov/eos_homepage/for_scientists/atbd/docs/MISR/atbd-misr-04.pdf

Jovanovic, V., Bull, M., Smyth, M., & Zong, J. (2002). MISR in-flight camera geometric model calibration and georectification performance. *IEEE Transactions on Geoscience and Remote Sensing*, *40*(7), 1512–1519.

Lewicki, S., Chafin, B., Crean, K., Gluck, S., Miller, K., & Paradise, S. (1999). MISR data products specifications. JPL Technical Report. http://eosweb.larc.nasa.gov/PRODOCS/misr/readme/dps_ne_icd.pdf

Loeb, N., & Davies, R. (1996). Observational evidence of plane parallel model biases: apparent dependence of cloud optical depth on solar zenith angle. *Journal of Geophysical Research, 101*, 1621–1634.

Menzel, P., Baum, B., Strabala, K., Frey, R. 2002. Cloud top properties and cloud phase ATBD, ATBD-04, version 6, September. Available at http://modis.gsfc.nasa.gov/data/atbd/atbd_mod04.pdf

Moroney, C., Davies, R., & Muller, J. -P. (2002). Operational retrieval of cloud-top heights using MISR data. *IEEE Transactions on Geoscience and Remote Sensing, 40*, 1532–1540.

Seiz, G. 2003. Ground- and satellite-based multi-view determination of 3D cloud geometry. PhD thesis, Institute of Geodesy and Photogrammetry, ETH Zürich, Switzerland, 2003. IGP Mitteilungen Nr. 80. Available at http://e-collection.ethbib.ethz.ch/cgi-bin/show.pl?type=diss and nr=15172

Seiz, G., Davies, R., Gruen, A. (accepted for publication). Stereo cloud-top height retrieval with ASTER and MISR. *Int. J. Rem. Sens.*

Snyder, J. (1987). Map projections—a working manual. *Technical report. USGS Professional, Vol. 1395.*

Wallis, R. (1976). An approach to the space variant restoration and enhancement of images. *Proc. of symp. on current mathematical problems in image science, naval postgraduate school, Monterey CA, USA, November.*

Yamaguchi, Y., Kahle, A., Tsu, H., Kawakami, T., & Pniel, M. (1998). Overview of Advanced Spaceborne Thermal Emission and Reflection Radiometer (ASTER). *IEEE Transactions on Geoscience and Remote Sensing, 36*, 1062–1071.

Zuidema, P., Davies, R., & Moroney, C. (2003). On the angular radiance closure of tropical cumulus congestus clouds observed by the multiangle imaging spectroradiometer. *Journal of Geophysical Research, 108*(D20), 4626. doi:10.1029/2003JD003401.